The effect of prestress force magnitude and eccentricity on the natural bending frequencies of prestressed concrete structures

Darragh Noble[a,*], Dr. Maria Nogal[a], Dr. Alan O'Connor[a], Dr. Vikram Pakrashi[b]

[a]*Dept. of Civil, Structural & Environmental Engineering, Museum Building, Trinity College Dublin, College Green, Dublin 2, Ireland.*
[b]*Dynamical Systems & Risk Laboratory, Civil & Environmental Engineering, School of Engineering, University College Cork, College Road, Cork, Ireland.*

Abstract

This paper describes the outcome of static 3-point bending testing and output-only experimental modal analysis on 9 post-tensioned concrete beams. Static 3-point bending testing and dynamic impact testing were conducted on each of the 9 beams at different levels of post-tensioning force. The Fast Fourier Transform (FFT) was implemented on the dynamic accelerometer impact data, and the fundamental frequencies of the simply supported post-tensioned concrete beams were determined by a peak-picking algorithm at each post-tensioning load level. The tests were repeated 10 times at each impact location to ensure repeatability of the experiment. There were 3 impact locations per post-tensioning load level, and there were 11 post-tensioning load levels at which the beams were tested. A first-order linear regression model was then applied to the measured fundamental bending frequencies with increasing post-tensioning load. Statistical significance tests were subsequently conducted on the recorded data to determine if any statistically significant changes in fundamental bending frequency with increasing post-tensioning load was observed, for both static and dynamic results. The results obtained for the static 3-point bending tests were then compared and contrasted with the results obtained from dynamic testing. No statistically significant relationship between natural frequency and post-tensioning load level was found

*Corresponding author
Email address: nobleda@tcd.ie (Darragh Noble)

for these uncracked concrete beams.

Keywords: Output-only, Experimental modal analysis, Post-tensioned concrete, Linear regression modelling, Fundamental bending frequency, 3-point bending tests.

1. Introduction

The prediction of the change in natural vibration frequencies with varying prestress force magnitude for prestressed concrete (PSC) structures is a particularly important problem. It has implications in the field of PSC bridge girders and for post-tensioned concrete wind turbine towers, both of which are structures that are susceptible to extreme dynamic excitation. The effect of applied prestressing force on the dynamic behaviour of pre- and post- tensioned structures is a widely debated topic [1]. Some authors argue that the natural vibration frequencies of PSC structures tend to decrease as the magnitude of the pre-stressing force is increased. This is known as the *"compression-softening"* effect and is based on Euler-Bernoulli beam theory of an externally axially loaded homogeneous beam [2, 3, 4, 5, 6, 7]. Others [8, 9] suggest that the natural frequencies of PSC structures are unaffected by pre-stress force magnitude. This argument has been taken to the fore by Hamed & Frostig [10], who present a non-linear kinematic model and conclude that the final equation of motion for the vibrating beam system is independent of the prestress force magnitude. Finally, there is also the argument that the NFs of PSC structures tend to increase as the magnitude of the pre-stressing force is increased. This was found to be the case in numerous empirical studies, conducted [11, 12, 13]. A satisfactory mathematical model predicting the increase in NFs with increasing pre-stressing force has yet to be formulated, despite some attempts [13, 14]. A comprehensive review of these models and studies has been outlined in previous works [15]. Prestress force decreases over time due to concrete creep, steel relaxation, anchorage pull-in and other factors. Structural engineers should thus be able to monitor or estimate changes in the natural bending frequency of PSC structures over the course of their design life to ensure their safety and serviceability. As a result, prediction of change in natural frequency of PSC structures over time is of great importance.

The aim of this paper is to report on results of both static and dynamic testing on post-tensioned concrete beams. The purpose of the research is

to determine the relationship between post-tensioning force magnitude and fundamental bending frequency for post-tensioned concrete beams. This paper is loosely based on the results and findings that have been previously presented by the authors [16, 17], and reference should be made to these articles for further information.

The novelty of this paper lies in the statistical significance testing of the results. Numerous other papers have been presented reporting correlation between natural frequency and post-tensioning load magnitude [11, 14, 3, 5, 12], but none have reported on the statistical significance of their results. Furthermore, this paper reports on the results of 9 beams, each with a different straight-profiled post-tensioning strand eccentricity, and as such the effect of post-tensioning strand eccentricity on natural bending frequencies of post-tensioned concrete beams is also determined. Finally, the post-tensioned concrete beams tested were verified as uncracked sections, unlike the specimens tested in previous studies [11].

This paper is organised as follows; Section 2 describes the set-up of two experiments in the laboratory. The first experiment is a static 3-point bending tests conducted on 9 post-tensioned concrete beams at different levels of post-tensioning force magnitude. The second experiment is a dynamic impact test, conducted on the same 9 beams, at the same post-tensioning load levels. Section 3 outlines the analysis of the results from both static and dynamic test regimes. Also, it outlines the prediction of the fundamental bending frequency of the beam sections, and describes the extensive signal-processing regime that was designed and implemented for the dynamic signals obtained. Section 4 describes the results of the static and dynamic experiments conducted, and compares the outcomes of both sets of experiments. Section 5 summarises the paper, drawing some significant conclusions and describes future work to be conducted. Appendix A outlines the detailed statistical parameters determining the statistical significance of the data collected and presented in Section 4.

2. Experimental Set-Up

2.1. Static 3-point bending tests

Three point static bending tests were conducted on post-tensioned concrete beams in the laboratory, as shown in the schematic in Figure 1. 9 post-tensioned concrete beams were tested statically through three point bending.

The 9 beams each had a different straight-profiled post-tensioning strand eccentricity, as outlined in Figure 4. The beams were placed underneath a small loading frame, rated to 180 tons, in the laboratory, anchored onto a metre deep reinforced concrete strong-floor. The loading ram was placed at midspan of the beam as shown in Figure 1. The loading ram was attached to a hydraulic jack, which was controlled via hand pump. The beams themselves are 2.3m long post-tensioned concrete beams with minimum reinforcement provided, in accordance with Eurocode 2 [18]. The span length between the simple supports was 2m. The beams were 200mm deep and 150mm wide in cross-section. The concrete had a characteristic strength, $f_{ck} = 30MPa$, which was determined from strength testing conducted on concrete cube specimens. The Young's Modulus of the concrete was determined experimentally to be $E_c = 26.88GPa$ from testing on standard concrete cylinders. The beams were lightly reinforced with 2 H12 as bottom reinforcement and 2 H8 as hanger bars (top reinforcement). H8 shear links were provided at 200mm centres and an additional 2 H8 shear links were provided in the anchorage zone as bursting reinforcement, in accordance with the CIRIA method, and as shown in Figure 1. Cover to all reinforcement was specified to be a minimum of 25mm [16, 17].

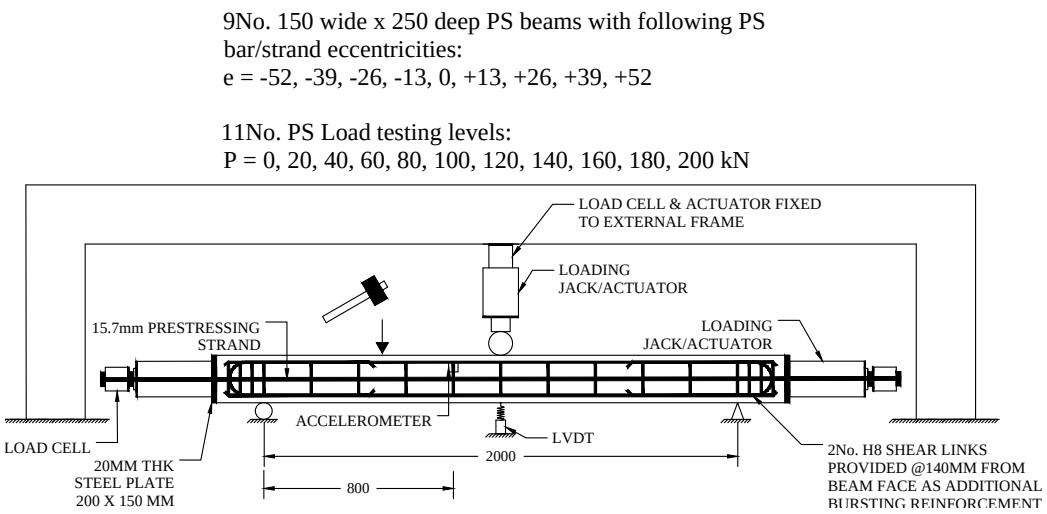

Figure 1: Experimental set-up.

A 15.7mm diameter 7-wire concentric Freyssinet pre-stressing strand, with a yield strength, f_y=1880MPa was threaded through a 20mm diam-

eter post-tensioning duct, cast into the concrete beam. 20mm steel plates were placed on either end of the beam. A 300 ton loading jack was placed on end against the steel plate. A TML KCM-300KNA *'through-hole compression'* load cell, rated to 300kN, was placed between loading jack and the prestressing collet. This arrangement was identical on each end of the beam, which helped to balance the mass on either end of the beam. A prestressing collet was fixed on the prestressing strand, such that when the jacks were elongated, they jacked against the prestressing collet, gripping the strand and hence, post-tensioning the concrete beam [16, 17]. The jack was controlled by means of a hydraulic hand pump.

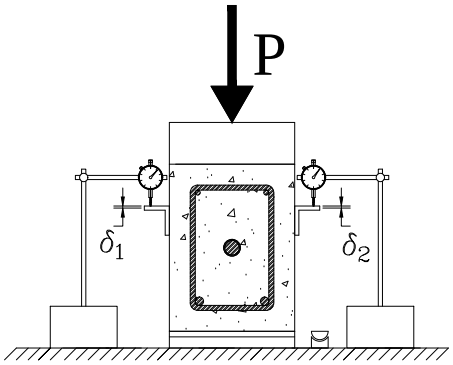

Figure 2: Measuring static deflection.

Each of the 9 concrete beams were tested statically at different values of post-tensioning load. The post-tensioning load levels were incremented in 20kN increments from 0-200kN. The lateral load was applied to the beams in such a way that the deflection reading from the dial gauges was never greater than 1mm, giving a minimum span/deflection ratio of 2000, much greater than the code specified value of 250. In this way, the test was deflection controlled. Furthermore, at such small values of midspan deflection, flexural cracking was not induced in any of the sections. Deflection was measured by means of two right-angled steel plates that were affixed to the beam section at mid-span as shown in Figure 2. A measurement was taken at each beam face to account for possible torsion of the beam section due to an asymmetrically applied load. Two deflection and transverse load readings were taken at each beam face, at each post-tensioning load level. This iteration was repeated once in order to minimize error in the experiment.

The results of the static testing are presented and discussed in Section 4.1, and the results presented in Table 2, and Figures 9 and 10.

2.2. Dynamic impact tests

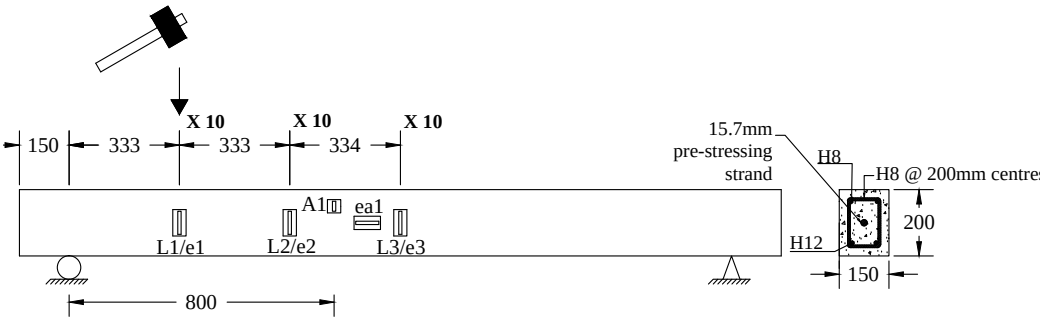

Figure 3: Instrumentation and set-up of dynamic test in laboratory

Dynamic impact testing was conducted on 9 post-tensioned concrete beams. Figure 1 in conjunction with Figure 3 shows the experimental set-up. Dynamic impact testing was conducted at three locations along the length of the beam span, as outlined in Figure 3, labelled L1-L3. The beam was struck 10 times at each location using an impact rig assembled in the lab with a rope and pulley system. A Dytran model 3200b4 10,000g range accelerometer was affixed to each of the beams tested. The accelerometer, 2 load cells and 4 strain gauges were connected to a System 6000 data logging system. The data was sampled at a rate of 10,000Hz, ensuring a Nyquist frequency of 5,000Hz. Since the fundamental bending frequency was expected to be approximately 78Hz, this sampling rate theoretically enabled the first 8 bending modes of vibration to be detected by the instrumentation (i.e. $78 \times 8^2 = 4,992$ Hz). The experiment was repeated at different post-tensioning load levels, as outlined in Figure 1. The post-tensioning load was increased in intervals of 20kN from 0-200kN. This helped ensure repeatability of the experiment. Strain gauges were fixed at the three impact locations (e1- e3) in order to obtain the mode shapes of vibration. The accelerometer (A1) was strategically placed at a distance of 800mm from the support, in order to identify all of the first three modes of vibration. Placement at midspan would eliminate the opportunity to obtain the second mode of vibration as it is a nodal point for the second mode. A fourth strain gauge (ea1) was placed in the axial direction, close to

midspan, in order to compare the axial strain data with the pre-stress load data obtained from the load cells [16, 17].

Figure 4 shows the cross-sections of each of the 9 post-tensioned concrete beams tested. Each beam has a different post-tensioning strand eccentricity, as shown.

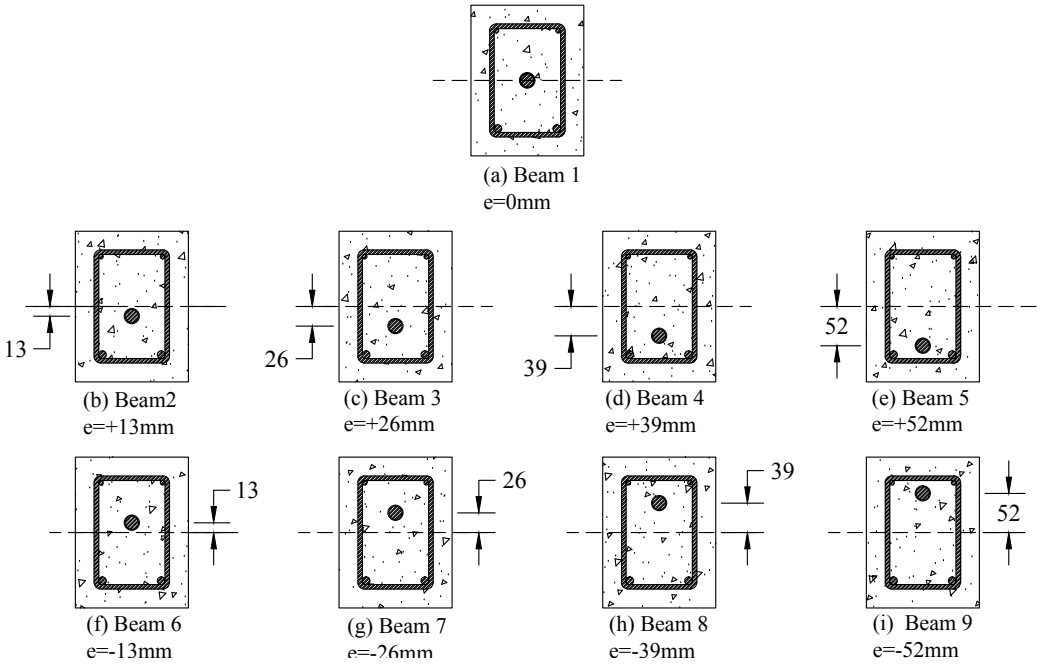

Figure 4: Cross sections of 9 beams tested.

3. Experimental Analysis

3.1. Prediction of the natural bending frequency

The prediction of the fundamental bending frequencies of each of the 9 uncracked and cracked post-tensioned concrete beams for zero post-tensioning force magnitude are outlined in Table 1. An uncracked analysis and cracked analysis of the post-tensioned concrete beams has been compared for zero post-tensioning force. The effect of the post-tensioning force itself should act as to increase the neutral axis depth and subsequently increase the frequency of vibration, where cracking has occurred. The frequencies have been predicted in accordance with Equation 2;

Table 1: Predictions of cracked and uncracked fundamental frequencies for PSC Beams

e (mm)	x_u (mm)	x_c (mm)	I_u (mm^4)	I_c (mm^4)	$\omega_{1,u}$ (Hz)	$\omega_{1,c}$ (Hz)
-52	99.58	49.37	1.116×10^8	8.847×10^7	79.26	70.58
-39	100.05	51.06	1.101×10^8	8.927×10^7	78.74	70.90
-26	100.53	52.71	1.091×10^8	9.040×10^7	78.37	71.35
-13	101.01	54.33	1.084×10^8	9.187×10^7	78.14	71.93
0	101.49	55.91	1.082×10^8	9.368×10^7	78.05	72.63
+13	101.96	57.47	1.083×10^8	9.585×10^7	78.10	73.47
+26	102.44	58.99	1.089×10^8	9.838×10^7	78.30	74.43
+39	102.92	60.49	1.098×10^8	1.013×10^8	78.64	75.51
+52	103.40	61.97	1.112×10^8	1.045×10^8	79.12	76.72

3.2. Analysis of Dynamic data

The signal processing regime followed the algoritm previously outlined in [15, 16, 17, 19]. The raw signal data contained significant noise and unwanted frequency content that corrupted the signal, meaning the dynamic characteristics such as natural frequency and damping were difficult to determine. The implementation of this algorithm ensured that a peak picking algorithm was able to identify the peaks in the frequency domain. Sample results can be seen in Figure 5. The peak picking method is the simplest means of determining the modal characteristics in the frequency domain, in which the natural frequencies correspond to the peaks in the FFT, however as pointed out in [20] *"this method is not reliable when the different modes of vibration are not sufficiently separated from each other."*

The search bands for the fundamental frequency of each beam were defined as 55-85Hz [17]. This algorithm is required to deal with the high levels of noise associated with impact testing of concrete beams with a relatively high fundamental bending frequency, which is expected to be in the region of 78Hz [17]. Figure 6 shows a flow chart diagram of the algorithm implemented for signal processing of the concrete beam specimens.

Figure 7 shows a typical accelerometer response a post-tensioned concrete beam. Figure 7a and 7b show the accelerometer signals in both the time and frequency domain, before the signal was processed to eliminate noise and after signal processing. The scale of the acceleration axis in the time domain

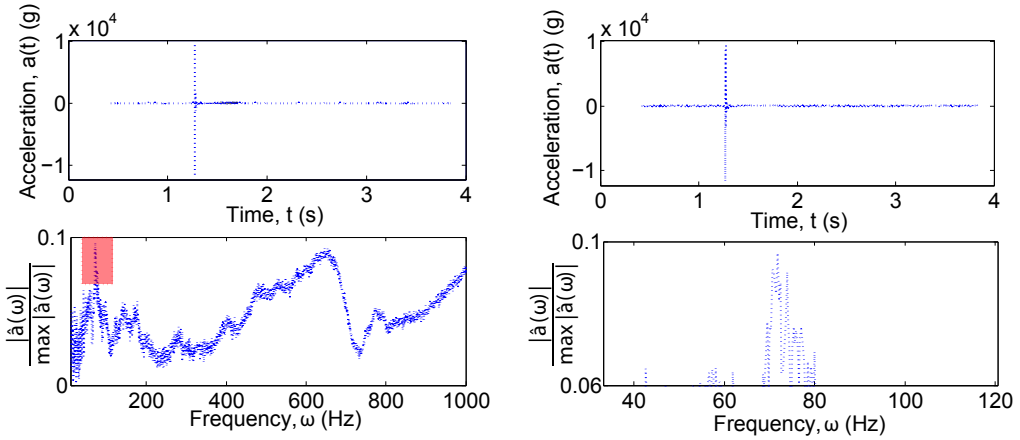

(a) (b)

Figure 5: Unprocessed, noisy signal at different scales (a) and (b). Identification of fundamental bending frequency possible. Higher modes unintelligible.

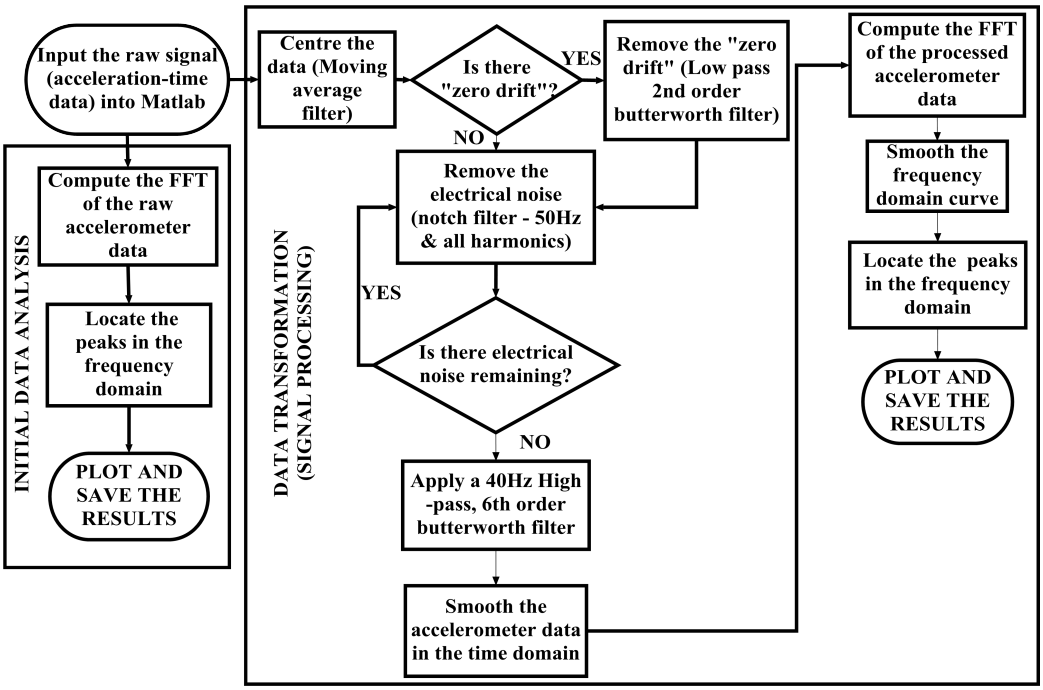

Figure 6: Signal processing algorithm flow chart.

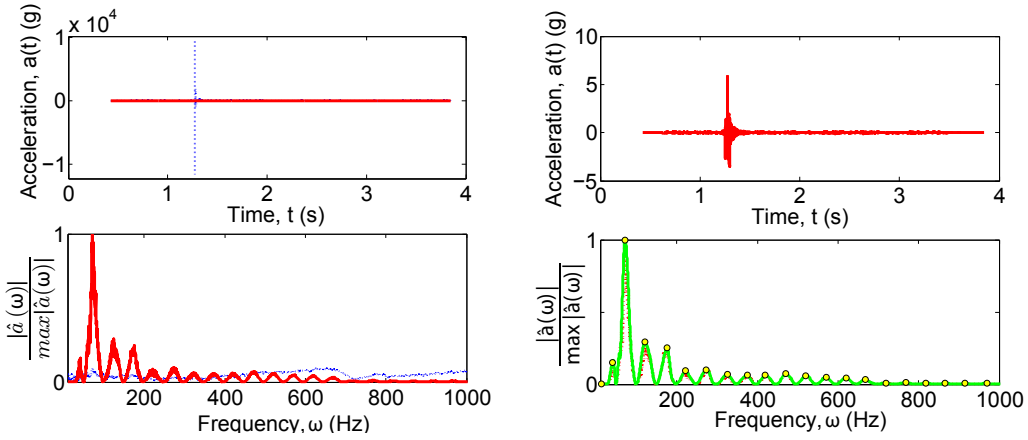

(a) (b)

Figure 7: (a) Signal Processing and (b) Peak Picking to identify correct fundamental bending frequencies.

of each signal is significantly reduced following signal processing, indicating the extent of the amplitude attributable to noise components [17].

3.3. Calculation of Damping Ratio, ξ

The damping ratio, ξ of the 9 concrete beams were calculated for each axial load level using the half-power bandwidth method, in the same way described by the authors in previous works [15]. The half-power bandwidth method enables evaluation of damping from forced vibration tests without knowing the applied force, and is thus used in vibration and modal testing. By assuming that the damping ratio ξ is small and that the frequency at maximum amplitude is approximately equal to the undamped fundamental frequency ω_1, the classical result relating the damping ratio to the half-power bandwidth can be written as [21];

$$\xi = \frac{\omega_b - \omega_a}{2\omega_1} \tag{1}$$

ω_a and ω_b are the half-power frequencies (i.e. the frequencies of the function at Max. Amplitude/$\sqrt{2}$). According to Wu [21], the classical result is only valid for damping ratio less than 0.1, and is not a good prediction for $\xi > 0.1$. An example of the calculation of the damping ratio in accordance by the half-power bandwidth method is shown in Figure 8.

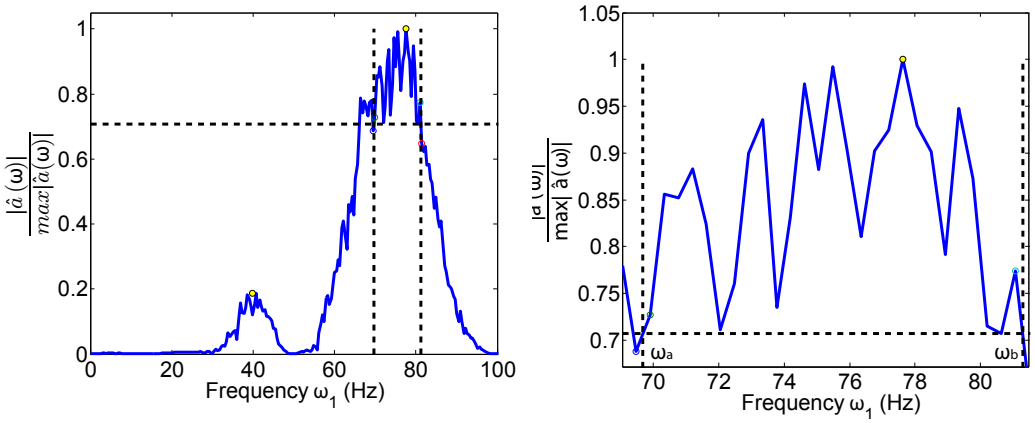

(a) (b)

Figure 8: Half-power bandwidth method of calculation of damping ratio, ξ

4. Experimental Results

4.1. Static Results

Static three-point bending tests were conducted on all 9 post-tensioned concrete beams. The post-tensioning force magnitude was varied and a point load was applied at midspan to the simply-supported post-tensioned concrete beam. The deflection corresponding to each transverse point load was measured, as described in Section 2.1 previously. A sample set of results are displayed in Table 2. From the collected load-deflection data, the equivalent static flexural rigidity, EI was estimated using the equation for deflection at midspan of a simply-supported beam due to a point-load applied at mid-span, $EI = \frac{P\ell^3}{48\delta}$, where P is the transverse load applied at mid-span, δ is the subsequent midspan deflection due to the applied point load, ℓ is the beam span length, E is the Young's Modulus of Elasticity, and I is the second moment of area of the cross section. The equation for the n^{th} natural bending frequency of a simply-supported beam is given as;

$$\omega_n = \left(\frac{n\pi}{\ell}\right)^2 \sqrt{\frac{EI}{m}} \tag{2}$$

where n is the mode number. In order to obtain a predicted static-equivalent bending frequency, $\omega_{n,S}$ the following substitution is made;

$$\omega_{n,S} = \left(\frac{n\pi}{\ell}\right)^2 \sqrt{\frac{P\ell^3}{48\delta m}} \tag{3}$$

This transformation from equivalent static flexural rigidity to fundamental natural bending frequency (i.e. $n = 1$) is given for Beam 1 (e=0mm) in Figure 9. Sample data for Beam 3 (e=+26mm) is given below in Table 2. The difference between the deflection data on either beam face is significant in this instance, highlighting the extent of the error in the experiment.

Table 2: Sample static data for Beam 3 (e=+26mm)

N (kN)	P (kN)	δ_1 (mm)	δ_2 (mm)	EI_1 $(kNmm^2)$	EI_2 $(kNmm^2)$	EI_{ave} $(kNmm^2)$	$\omega_{1,S_{ave}}$ (Hz)
0.15	10.1	0.80	1.00	2.10E+09	1.68E+09	1.89E+09	63.08
0.16	10.5	0.79	1.00	2.22E+09	1.75E+09	1.98E+09	64.54
23.06	10.6	0.64	1.00	2.76E+09	1.77E+09	2.26E+09	68.96
23.00	10.7	0.63	1.00	2.83E+09	1.78E+09	2.31E+09	69.62
44.53	11.3	0.53	1.00	3.55E+09	1.88E+09	2.72E+09	75.58
44.39	11.5	0.55	1.00	3.48E+09	1.92E+09	2.70E+09	75.33
63.07	12.5	0.47	1.00	4.43E+09	2.08E+09	3.26E+09	82.74
62.95	12.5	0.48	1.01	4.34E+09	2.06E+09	3.20E+09	82.02
82.34	13.7	0.44	1.01	5.19E+09	2.26E+09	3.73E+09	88.47
82.26	13.4	0.44	1.00	5.08E+09	2.23E+09	3.65E+09	87.63
100.69	14.1	0.40	1.00	5.88E+09	2.35E+09	4.11E+09	92.96
100.72	14.5	0.43	1.01	5.62E+09	2.39E+09	4.01E+09	91.75
121.04	15.2	0.41	1.00	6.18E+09	2.53E+09	4.36E+09	95.67
120.77	15.3	0.40	1.00	6.38E+09	2.55E+09	4.46E+09	96.83
141.48	15.8	0.34	1.00	7.75E+09	2.63E+09	5.19E+09	104.42
141.31	15.7	0.40	1.00	6.54E+09	2.62E+09	4.58E+09	98.09
161.64	16.0	0.39	1.00	6.84E+09	2.67E+09	4.75E+09	99.92
161.20	16.4	0.40	1.00	6.83E+09	2.73E+09	4.78E+09	100.25
179.96	16.8	0.38	1.02	7.37E+09	2.75E+09	5.06E+09	103.08
179.49	16.5	0.36	1.00	7.64E+09	2.75E+09	5.19E+09	104.47
202.42	16.9	0.38	1.02	7.41E+09	2.76E+09	5.09E+09	103.38
201.54	16.7	0.37	1.00	7.52E+09	2.78E+09	5.15E+09	104.05

Figure 9a shows the measured change in static flexural rigidity, EI with increasing post-tensioning force magnitude for Beam 1 (e=0mm), and Figure 9b shows the equivalent static prediction of the fundamental bending

frequency using Equation 3. Figure 10 shows the static prediction of natural bending frequency based on the measured 3-point bending data for all 9 post-tensioned concrete beams for varying post-tensioning force magnitude. In the case of Beams 1-6, a statistically significant increasing trend is observed in predicted static-equivalent fundamental bending frequencies with increasing post-tensioning force. In the case of Beams 2-5, the effect of the post-tensioning strand eccentricity is to cause the beams to camber upwards and the downward deflection to be reduced. The greater the magnitude of the post-tensioning load, the greater the magnitude of midspan point load required to induce 1mm deflection, and, as such, the static flexural rigidity, and hence the natural bending frequency is predicted to increase. In the case of Beams 6-9, the effect of the post-tensioning strand eccentricity is such as to induce further cracking in the bottom fibre and cause further sagging in the simply supported beam, therefore a lesser magnitude of midspan point load would be required to induce the 1mm deflection, and therefore, the static flexural rigidity, and hence the natural bending frequency is predicted to decrease. Beam 1 (e=0mm) has zero eccentricity, and therefore no moment due to prestressing force. In this case, the axial normal stress acts so as to ensure the entire section acts in pure compression, significantly increasing its capacity to resist transverse load before cracking occurs in the bottom fibre of the section.

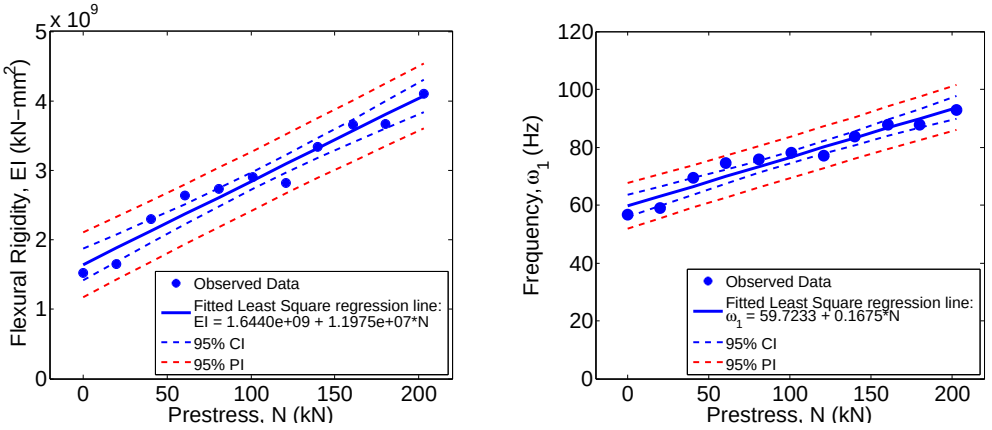

Figure 9: (a) Beam 1 (e=0mm); Static, EI (b) Beam 1 (e=0mm); Dyn. equiv. ω_1

For Figure 10, when examined in conjunction with Table A.3, which presents the results of the statistical analysis conducted on the regression parameters for regressing $\omega_{1,s1}$ and $\omega_{1,s2}$ respectively on N, it is determined that for Beam 1-6, a statistically significant increase in static-equivalent natural bending frequency with increasing post-tensioning load magnitude is apparent. However, for Beam 7-9, no statistically significant trend can be identified in the data. This is concurrent with what was predicted due to the different stress distributions in the given sections. Beam 7-9 have eccentricities that promote further bending and cracking in the bottom fibre, and hence increasing the post-tensioning load acts as to open cracks and theoretically decrease the bending frequency. This has not been found experimentally. At best, from this data, a non-significant statistical trend is all that can be observed.

These static-equivalent bending frequencies shall be compared against the measured natural bending frequencies obtained from dynamic impact testing on the same post-tensioned concrete sections in Section 4.3.

4.2. Dynamic Results

Figure 11 shows sample results for Beam 2 (e=+13mm). Figure 11a shows the peaks of the frequency domain representation of all 30 signals superimposed on each other for each post-tensioning load level. In total, there are 330 signals superimposed in the graph. The dominance of the fundamental bending mode of vibration is evident from this figure, due to the relative contribution of this mode to the overall structural dynamic response of the system. This dominance of the first bending mode was observed for all 9 beams tested. The vertical axis shows the normalised relative modal amplitude of the response of the system. Figure 11b represents Figure 11a in two dimensions. The diameter of the data points is directly proportional to the relative modal amplitude. All peaks in the frequency domain in the range of 0-1000Hz are plotted against the post-tensioning load level of the tested specimen. The fundamental bending frequency has been identified to lie within the search bands of 55 to 85Hz. Figure 11c zooms in on Figure 11b and shows the estimation of the first modal frequency from peak picking of each of the 330 dynamic signals obtained, at different post-tensioning load levels. The scatter in the estimation of the fundamental frequency is noted to be large. Figure 11d shows some simple data analytics. The standard deviation, σ of the data ranges between 2 and 4Hz, which is between 3 and 5% of the mean, μ of each data set [17].

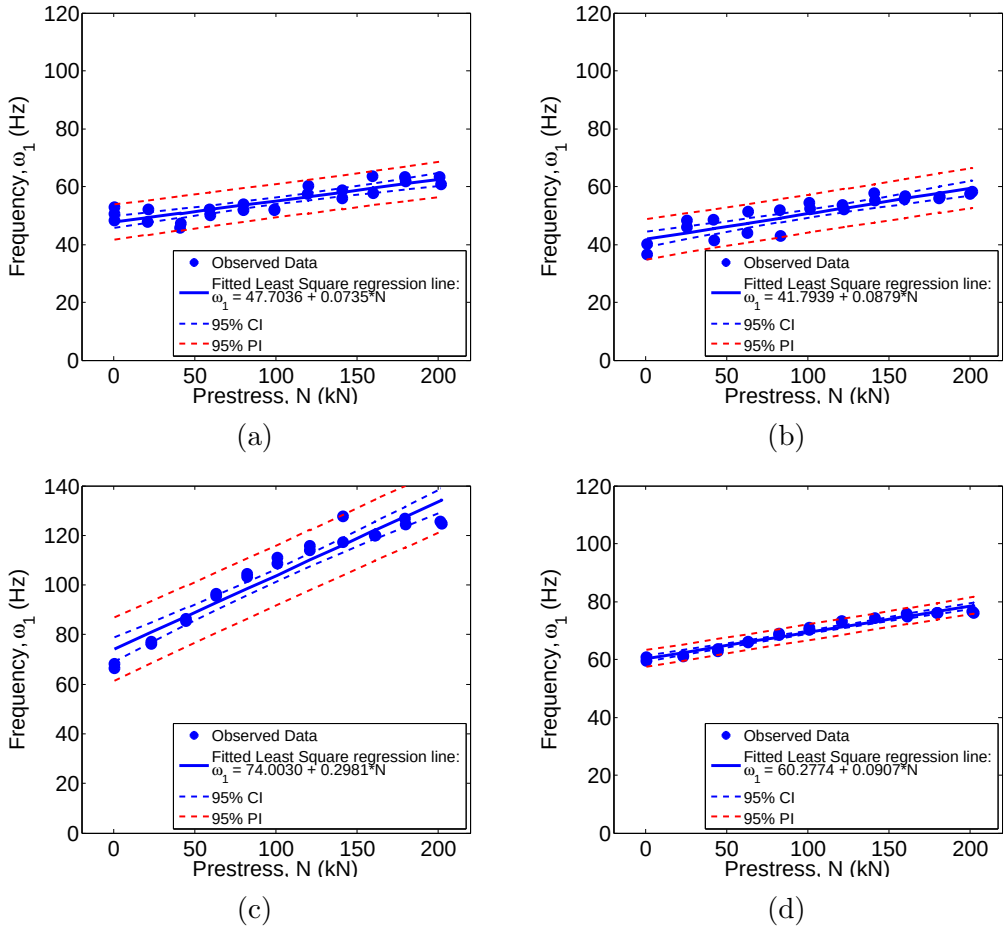

Figure 10: (a) Beam 2 (e=+13mm); Iteration 1 (b) Beam 2 (e=+13mm); Iteration 2; (c) Beam 3 (e=+26mm); Iteration 1 (d) Beam 3 (e=+26mm); Iteration 2

4.2.1. 3D Graphs

Figure 12 show 3D graphs of normalised relative modal amplitude of the response of the system versus frequency and post-tensioning load level. As can be seen in each of the graphs, the dominance of the first bending mode of vibration in the overall structural dynamic response of the system is apparent. Figure 12a shows the frequency response of Beam 2 (e=+13mm) for each axial load level. Figure 12b shows the frequency response of Beam 3 (e=+26mm) which has a post-tensioning strand eccentricity that promote

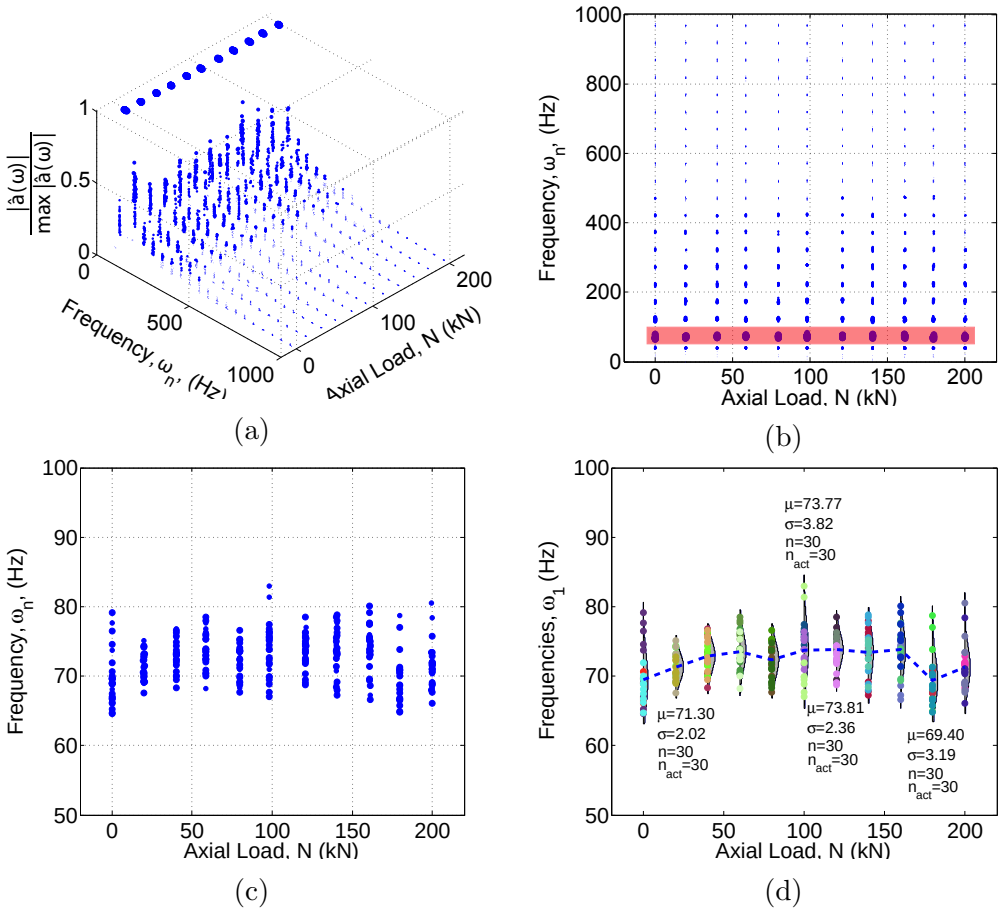

Figure 11: (a) Processed signals in frequency domain as a function of axial load (3D); (b) All modes plotted against axial load (2D); (c) Zooming in on the fundamental bending frequency; (d) Simple data analytics on the measured frequencies as a function of axial force (Beam 2).

upward camber and compression in the bottom fibre of the section. The importance of these graphs is that they highlight the dominance of the first bending mode of vibration in the overall structural dynamic response. This has been observed for all 9 post-tensioned concrete beams tested in the laboratory.

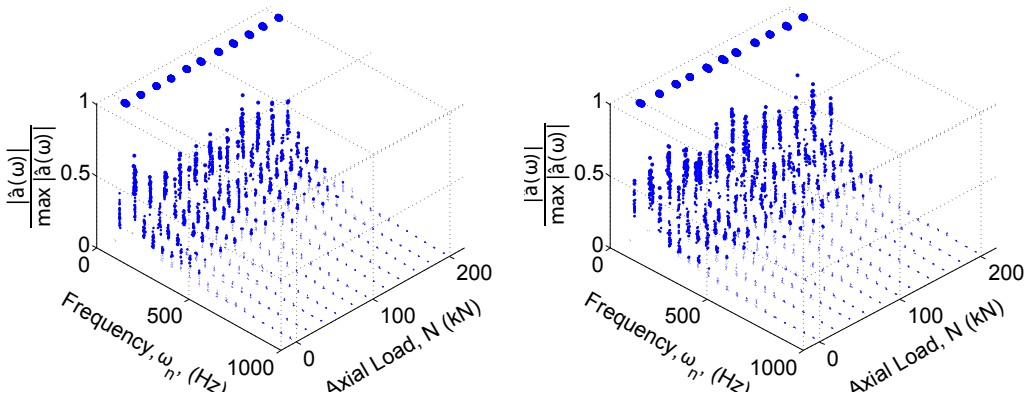

Figure 12: (a) Beam 2 (e=+13mm); (b) Beam 3 (e=+26mm).

4.2.2. Regression Analysis

Figures 15 shows the results of a linear regression analysis that has been applied to the relationship between the fundamental bending mode of vibration and the post-tensioning load level. The results for Beam 2 have been published previously [17], but this paper expands on previous studies and reports on results for a whole suite of 9 post-tensioned concrete beams. The smaller data points represent each individual estimation of the fundamental frequency, while the larger data points represent the mean of each data set. The inner dashed line represents the 95% confidence interval for the regression line, while the outer dashed line is the 95% prediction interval for an individual estimation. The results of statistical t-test on the regression slope parameter, for each of the 9 beams tested, are displayed in Table A.4. It was found, for 6 of the 9 post-tensioned concrete beams (namely, Beams 1,2,3,4,6,9) that there is no statistically significant change in fundamental bending frequency with prestress force magnitude. 3 beams showed a statistically significant increase in fundamental bending frequency with increasing post-tensioning force magnitude (namely Beams 5,7,8). Furthermore, Figure 13 shows all data for Beam 2 plotted on a normal probability paper. All data points lie within the boundaries that would be expected if it were from the same, Normal parent distribution. This further indicates that any observed changes in natural frequency with post-tensioning load magnitude is likely due to chance rather than any systematic effect. Similar results have been observed for 6 of the 9 beams tested.

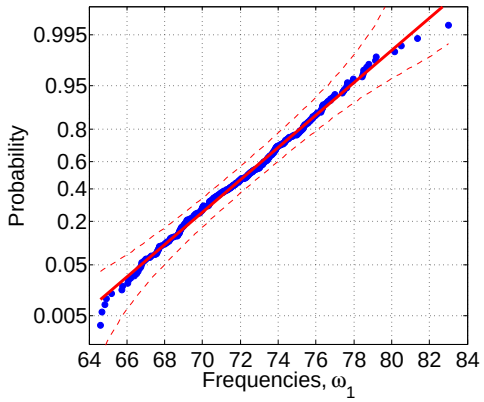

Figure 13: All data for Beam 2 (e=+13mm) plotted on a normal probability paper, indicating data normality.

As outlined in [17], Figure 14 shows a comparison of the different regression lines for each of the 9 beams plotted against one another. Figure 14a shows the results for Beams 1-5 while Figure 14b shows the results for Beam 1 and Beams 6-9. Theory would suggest that as the eccentricity increases, the intercept values of the regression lines should also increase, as there is increased second moment of area due to the parallel axis theorem, and a subsequent expected increase in *'virgin'* natural bending frequencies for the simply supported post-tensioned beams. However, as shown in Figure 14, according to the experimental results obtained, this is not the case. Statistically significant increases in natural frequency with increasing post-tensioning load were observed for Beam Nos. 5,7 & 8. All other beams displayed no statistically significant changes in natural frequency. This is outlined further in Table A.4.

Table A.4 shows the calculated linear regression intercept parameter ($\alpha_{0,i}$), and slope parameter ($\alpha_{1,i}$) when regressing ω_1 on N for all 9 beams (i). The corresponding linear regression equations are obtained by substituting into the following formula;

$$\omega_1 = \alpha_{0,i} + \alpha_{1,i} N \tag{4}$$

4.3. Static vs. Dynamic results

Figure 16 shows the comparison between the static-equivalent prediction of fundamental bending frequency to the measured frequencies from the

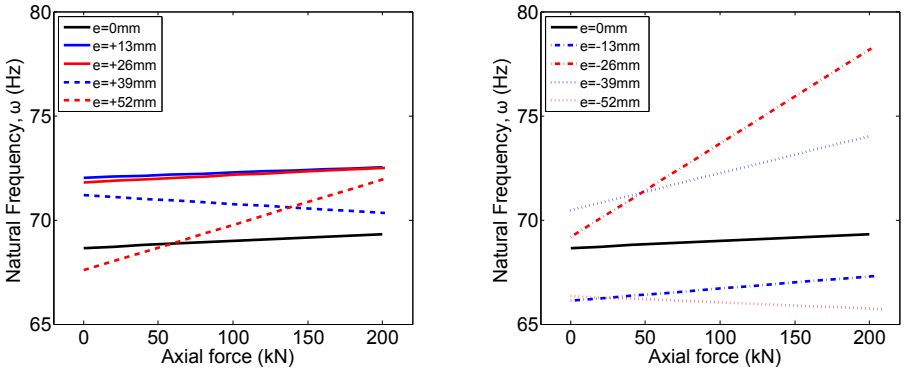

(a) (b)

Figure 14: Collated data of linear regression of fundamental bending frequency as a function of post-tensioning load for (a) Beams 1-5 and (b) Beams 1, 6-9.

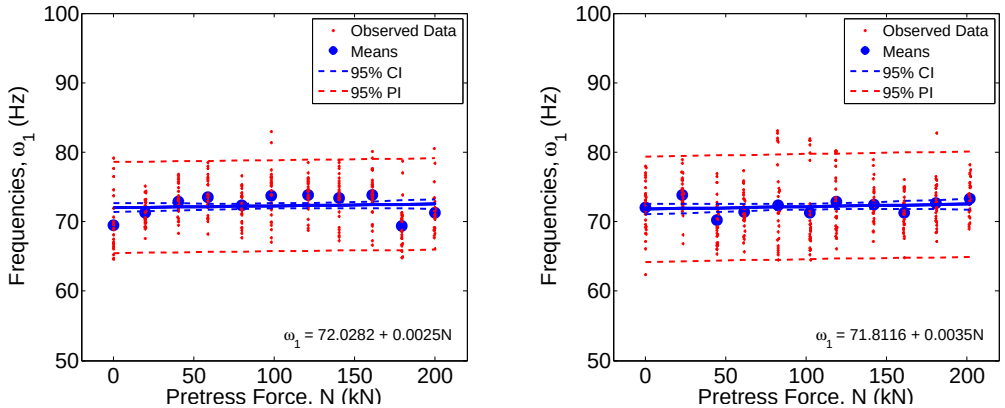

(a) (b)

Figure 15: Regression of ω_1 on N for; (a) Beam 2 (e=+13mm); (b) Beam 3 (e=+26mm).

dynamic data. The linear regression lines for both the static-equivalent predictions and the dynamic data are plotted against one another for Beams 2 & 3, as shown. For Beams 1,2,3,4,5,6 the static-equivalent prediction of fundamental bending frequency shows a statistically significant increase in the bending frequency with increasing post-tensioning force magnitude. However, in comparison, the results from the dynamic testing show no statisti-

cally significant trend in the data. For Beams 7,8 & 9, the static-equivalent data shows no statistically significant trend with increasing post-tensioning force magnitude.

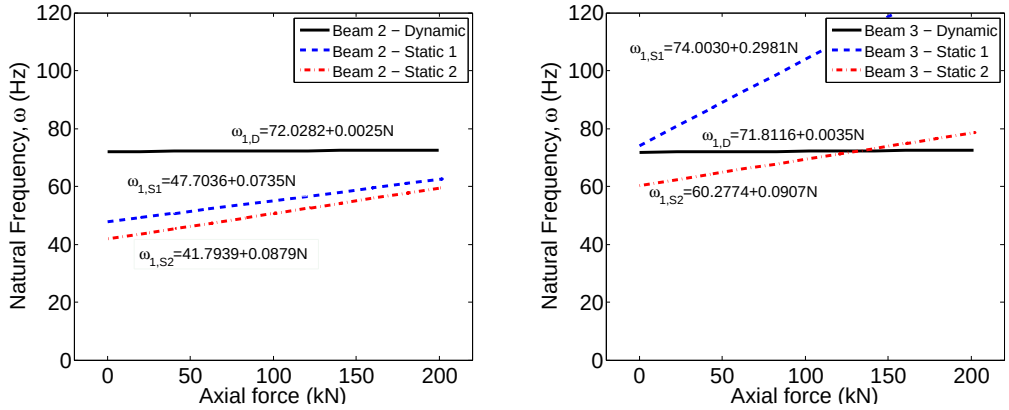

(a) (b)

Figure 16: Comparison of static and dynamic results; (a) Beam 2 (e=+13mm); (b) Beam 3 (e=+26mm).

4.4. Damping ratios

Figure 17 shows the results of a statistical regression analysis of calculated critical damping ratios versus post-tensioning force magnitude. Figure 17 should be analysed in conjunction with Table A.5, which outlines the statistical linear regression parameters, indicating the statistical significance of the changes observed in Figure 17. Beams 1,4 & 6 show no statistically significant relationship between damping ratio and post-tensioning load level. Beams 2,8 & 9 show a statistically significant decreasing trend in damping ratio with increasing post-tensioning load level, while Beams 3,5 & 7 show a statistically significant increasing trend in damping ratio with increasing post-tensioning load level. As such, the testing results are inconclusive. No definitive statement on the relationship between damping ratio and post-tensioning force magnitude can be made, based on the obtained results, as depending on the beam tested, different statistical significance conclusions have been observed. The value of the critical damping ratio measured ranges between 0.23-5.01%, which is in the range predicted for concrete structures.

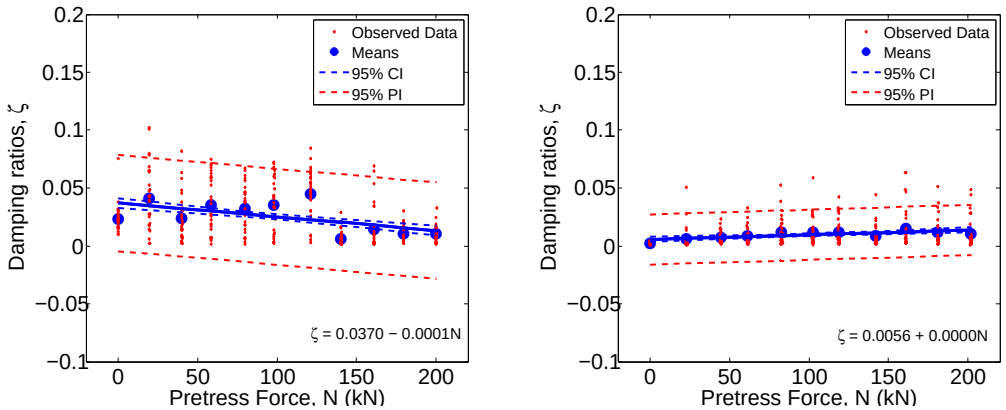

(a) (b)

Figure 17: Regression of ξ on N for; (a) Beam 2 (e=+13mm); (b) Beam 3 (e=+26mm).

5. Conclusions

The prediction of the change in natural bending frequencies with varying prestress force magnitude for PSC structures is an important problem, particularly in the field of PSC bridge girders and more recently for pre-cast, post-tensioned concrete wind turbine towers, both of which are structures that are susceptible to extreme dynamic excitation. Following this output-only modal analysis study, it was concluded that no statistically significant relationship was found between post-tension force magnitude and fundamental bending frequency for 6No. of 9No. simply supported post-tensioned concrete beams tested in the laboratory. The other 3No. beams displayed a statistically significant increase in fundamental bending frequency with increasing post-tensioning load.

The full conclusions of the study are outlined as follows;

1. The "compression-softening" effect is not valid for post-tensioned concrete structures. From the static and dynamic tests conducted, no evidence of a decreasing trend in fundamental bending frequency with increasing post-tensioning force magnitude has been found.

2. From the obtained static data, the static-equivalent prediction of the fundamental bending frequency suggests that there is an increasing

trend in fundamental bending frequency with increasing post-tensioning load magnitude.

3. However, from the obtained dynamic data, there is no indication of any relationship between post-tensioning load magnitude and fundamental bending frequency.

4. The dominance of the fundamental bending mode in the overall structural dynamic response of each of the 9No. post-tensioned concrete beams is evident from the 3D graphs produced.

5. The results are inconclusive regarding the relationship between the change in critical damping ratio, ξ and the post-tensioning force magnitude, N.

6. Despite theory predicting that there should be a direct relationship between post-tensioning strand eccentricity and fundamental bending frequency, no such non-random systematic change could be identified from the analysis of the obtained data.

Recently the interest on variability of dynamic properties of bridges (i.e. natural frequency, mode shape, damping ratio) caused by environmental effects such as temperature, humidity, wind and other factors is increasing [22]. Studies conducted [23, 24] report frequency differences in the ranges of 6% and 14-18% respectively due to normal environmental changes (e.g. temperature effects, lack of ideal support conditions, material variability etc...). The change in natural frequency due to prestress loss is therefore considered negligible in relation to such large environmental effects.

The main findings of this paper indicate that, for uncracked post-tensioned concrete sections, no statistically significant relationship has been found between post-tensioning force magnitude and natural bending frequency, as opposed to some research works [2, 3, 5, 6, 7, 11, 12, 13, 25, 26, 27], but falling in line with the results suggested by others [9, 8, 10, 28, 29, 30, 31]. The implication of this result is profound in system identification. Since the vast majority of pre- and post-tensioned concrete structures currently in service have not been instrumented for the magnitude of the post-tensioning force, it had been suggested that non-destructive testing methods could be used to identify the magnitude of the post-tensioning force, from the analysis of dynamic data. However, since no statistically significant relationship

could be determined between post-tensioning load magnitude and natural bending frequency, for uncracked post-tensioned concrete sections, it is not possible to determine the magnitude of the post-tensioning force from the natural frequency of uncracked pre- and post-tensioned concrete sections.

Acknowledgements

The authors would like to gratefully acknowledge the financial support donated by the Irish Research Council (IRC) under its Embark initiative. The authors would also like to sincerely thank Banagher Concrete, Heitons Steel, Roadstone Ireland, Fairyhouse Steel, and Freyssinet Ireland for their support in supplying testing materials throughout the duration of the project to date.

Appendix A.

Table A.4 shows the calculated linear regression intercept parameter (α_0), and slope parameter (α_1) when regressing ω_1 on N for all nine number beams (i). The corresponding linear regression equations are obtained by substituting into the following formula;

$$\omega_1 = \alpha_{0,i} + \alpha_{1,i} N \tag{A.1}$$

Table A.5 shows the calculated linear regression intercept parameter (β_0), and slope parameter (β_1) when regressing ξ on N for all nine number beams (i). The corresponding linear regression equations are obtained by substituting into the following formula;

$$\xi = \beta_{0,i} + \beta_{1,i} N \tag{A.2}$$

Table A.3: Statistical analysis on regression parameters for $\omega_{1,S1}$ and $\omega_{1,S2}$ on N

B#	Reg. P.	Value	SE	t-value	t-crit.	p	95% CI
B1	$\alpha_{0,1}$	59.7233	1.6972	35.19	2.2622	0.0000	(55.8840,63.5626)
	$\alpha_{1,1}$	0.1675	0.0142	11.76	2.2622	0.0000	(0.1353,0.1997)
	$\alpha_{0,1}$	58.7176	5.5784	10.53	2.2622	0.0000	(46.0984,71.3368)
	$\alpha_{1,1}$	0.2755	0.0468	5.88	2.2622	0.0002	(0.1696,0.3813)
B2	$\alpha_{0,2}$	47.7036	1.0101	47.22	2.0796	0.0000	(45.6029,49.8043)
	$\alpha_{1,2}$	0.0735	0.0087	8.44	2.0796	0.0000	(0.0553,0.0916)
	$\alpha_{0,2}$	41.7939	1.2572	33.24	2.0860	0.0000	(39.1716,44.4163)
	$\alpha_{1,2}$	0.0879	0.0105	8.36	2.0860	0.0000	(0.0660,0.1099)
B3	$\alpha_{0,3}$	74.0030	2.3010	32.16	2.0860	0.0000	(69.2032,78.8028)
	$\alpha_{1,3}$	0.2981	0.0193	15.48	2.0860	0.0000	(0.2579,0.3383)
	$\alpha_{0,3}$	60.2774	0.5241	115.01	2.0860	0.0000	(59.1841,61.3707)
	$\alpha_{1,3}$	0.0907	0.0044	20.69	2.0860	0.0000	(0.0816,0.0999)
B4	$\alpha_{0,4}$	66.8800	0.6230	107.35	2.0860	0.0000	(65.5804,68.1796)
	$\alpha_{1,4}$	0.1363	0.0052	26.04	2.0860	0.0000	(0.1253,0.1472)
	$\alpha_{0,4}$	64.1038	0.5541	115.70	2.0860	0.0000	(62.9481,65.2596)
	$\alpha_{1,4}$	0.1541	0.0047	33.06	2.0860	0.0000	(0.1444,0.1638)
B5	$\alpha_{0,5}$	66.5409	0.8758	75.98	2.0860	0.0000	(64.7140,68.3679)
	$\alpha_{1,5}$	0.1072	0.0073	14.67	2.0860	0.0000	(0.0919,0.1224)
	$\alpha_{0,5}$	63.8006	0.9855	64.74	2.0860	0.0000	(61.7448,65.8564)
	$\alpha_{1,5}$	0.1200	0.0082	14.64	2.0860	0.0000	(0.1029,0.1371)
B6	$\alpha_{1,6}$	61.3804	0.6625	92.65	2.0860	0.0000	(59.9984,62.7623)
	$\alpha_{1,6}$	0.0643	0.0055	11.61	2.0860	0.0000	(0.0528,0.0759)
	$\alpha_{1,6}$	58.8722	0.4548	129.46	2.0860	0.0000	(57.9237,59.8208)
	$\alpha_{1,6}$	0.0732	0.0038	19.22	2.0860	0.0000	(0.0653,0.0812)
B7	$\alpha_{0,8}$	66.7005	0.7977	83.62	2.0860	0.0000	(65.0366,68.3644)
	$\alpha_{1,8}$	-0.0005	0.0067	-0.07	2.0860	0.9462	(-0.0144,0.0135)
	$\alpha_{0,7}$	60.9159	0.4011	151.88	2.0860	0.0000	(60.0792,61.7525)
	$\alpha_{1,7}$	0.0189	0.0034	5.65	2.0860	0.0000	(0.0119,0.0259)
B8	$\alpha_{0,8}$	62.8552	0.4784	131.38	2.0860	0.0000	(61.8572,63.8532)
	$\alpha_{1,8}$	0.0073	0.0041	1.77	2.0860	0.9462	(-0.0013,0.0159)
	$\alpha_{0,8}$	57.7603	0.2238	258.10	2.0860	0.0000	(57.2935,58.2271)
	$\alpha_{1,8}$	0.0193	0.0019	10.31	2.0860	0.0000	(0.0154,0.0232)
B9	$\alpha_{0,9}$	63.1564	0.5440	116.10	2.0860	0.0000	(62.0216,64.2911)
	$\alpha_{1,9}$	-0.0012	0.0045	-0.27	2.0860	0.7921	(-0.0107,0.0083)
	$\alpha_{0,9}$	64.1017	0.9121	70.28	2.0860	0.0000	(62.1992,66.0043)
	$\alpha_{1,9}$	-0.0159	0.0077	-2.07	2.0860	0.0516	(-0.0319,0.0001)

Table A.4: Statistical analysis on regression parameters for $\omega_{1,D}$ on N

B#	Reg. P.	Value	SE	t-value	t-crit.	p	95% CI
B1	$\alpha_{0,1}$	68.6585	2.0515	33.4680	1.9672	0.0000	(64.6228,72.6942)
	$\alpha_{1,1}$	0.0033	0.0204	0.1635	1.9672	0.8702	(-0.0368,0.0434)
B2	$\alpha_{0,2}$	72.0282	0.3415	210.9027	1.9672	0.0000	(71.3563,72.7000)
	$\alpha_{1,2}$	0.0025	0.0029	0.8589	1.9672	0.3910	(-0.0032,0.0082)
B3	$\alpha_{0,3}$	71.8116	0.4017	178.7481	1.9672	0.0000	(71.0213,72.6020)
	$\alpha_{1,3}$	0.0035	0.0034	1.0310	1.9672	0.3033	(-0.0031,0.0101)
B4	$\alpha_{0,4}$	71.1915	0.3728	190.9584	1.9672	0.0000	(70.4581,71.9249)
	$\alpha_{1,4}$	-0.0043	0.0031	-1.3659	1.9672	0.1729	(-0.0104,0.0019)
B5	$\alpha_{0,5}$	67.6526	0.5805	116.5487	1.9672	0.0000	(66.5107,68.7946)
	$\alpha_{1,5}$	0.0211	0.0049	4.2831	1.9672	0.0000	(0.0114,0.0307)
B6	$\alpha_{1,6}$	66.1165	0.4804	137.6213	1.9672	0.0000	(65.1714,67.0616)
	$\alpha_{1,6}$	0.0059	0.0040	1.4877	1.9672	0.1378	(-0.0019,0.0138)
B7	$\alpha_{0,7}$	69.6030	0.3444	202.1280	1.9677	0.0000	(68.9254,70.2806)
	$\alpha_{1,7}$	0.0445	0.0029	15.4322	1.9677	0.0000	(0.0388,0.0502)
B8	$\alpha_{0,8}$	70.6975	0.3820	185.0695	1.9684	0.0000	(69.9456,71.4494)
	$\alpha_{1,8}$	0.0453	0.0038	11.9044	1.9684	0.0000	(0.0378,0.0528)
B9	$\alpha_{0,9}$	66.3616	0.6663	99.5991	1.9672	0.0000	(65.0509,67.6724)
	$\alpha_{1,9}$	-0.0032	0.0054	-0.5856	1.9672	0.5586	(-0.0137,0.0074)

Table A.5: Statistical analysis on regression parameters for ξ on N

B#	Reg. P.	Value	SE	t-value	t-crit.	p	95% CI
B1	$\beta_{0,1}$	0.0211	0.0096	2.2022	1.9672	0.0283	(0.0023,0.0400)
	$\beta_{1,1}$	0.0000	0.0001	0.1699	1.9672	0.8652	(-0.0002,0.0002)
B2	$\beta_{0,2}$	0.0370	0.0022	17.1074	1.9672	0.0000	(0.0327,0.0412)
	$\beta_{1,2}$	-0.0001	0.0000	-6.4672	1.9672	0.0000	(-0.0002,-0.0001)
B3	$\beta_{0,3}$	0.0056	0.0012	4.8365	1.9672	0.0000	(0.0033,0.0078)
	$\beta_{1,3}$	0.0000	0.0000	4.1999	1.9672	0.0000	(0.0000,0.0001)
B4	$\beta_{0,4}$	0.0338	0.0014	24.4342	1.9672	0.0000	(0.0311,0.0365)
	$\beta_{1,4}$	-0.0000	0.0000	-0.8902	1.9672	0.3740	(-0.0000,0.0000)
B5	$\beta_{0,5}$	0.0362	0.0021	16.9762	1.9672	0.0000	(0.0320,0.0404)
	$\beta_{1,5}$	0.0000	0.0000	2.5735	1.9672	0.0105	(0.0000,0.0001)
B6	$\beta_{1,6}$	0.0298	0.0013	22.4369	1.9672	0.0000	(0.0272,0.0324)
	$\beta_{1,6}$	-0.0000	0.0000	-0.0969	1.9672	0.9228	(-0.0000,0.0000)
B7	$\beta_{0,7}$	0.0366	0.0018	20.7348	1.9675	0.0000	(0.0332,0.0401)
	$\beta_{1,7}$	0.0001	0.0000	6.5090	1.9675	0.0000	(0.0001,0.0001)
B8	$\beta_{0,8}$	0.0469	0.0016	29.4815	1.9672	0.0000	(0.0438,0.0501)
	$\beta_{1,8}$	-0.0000	0.0000	-2.4571	1.9672	0.0145	(-0.0001,-0.0000)
B9	$\beta_{0,9}$	0.0420	0.0022	19.3577	1.9672	0.0000	(0.0377,0.0462)
	$\beta_{1,9}$	-0.0001	0.0000	-2.8821	1.9672	0.0042	(-0.0001,-0.0000)

References

[1] A. Quilligan, A. O'Connor, V. Pakrashi, Fragility analysis of steel and concrete wind turbine towers, Engineering Structures 36 (2012) 270 – 282.

[2] F. Tse, I. Morse, R. Hinkle, Mechanical vibrations: theory and applications, Allyn and Bacon series in mechanical engineering and applied mechanics, Allyn and Bacon, 1978.

[3] K. K. Raju, G. V. Rao, Free vibration behavior of prestressed beams, Journal of Structural Engineering 112 (1986) 433–437.

[4] A. Dall'Asta, G. Leoni, Vibrations of beams prestressed by internal frictionless cables, Journal of Sound and Vibration 222 (1) (1999) 1 – 18.

[5] A. Miyamoto, K. Tei, H. Nakamura, J. Bull, Behavior of prestressed beam strengthened with external tendons, Journal of Structural Engineering 126 (9) (2000) 1033–1044.

[6] T. Chan, T. Yung, A theoretical study of force identification using prestressed concrete bridges, Engineering Structures 22 (11) (2000) 1529 – 1537.

[7] S. Law, Z. Lu, Time domain responses of a prestressed beam and prestress identification, Journal of Sound and Vibration 288 (4-5) (2005) 1011–1025.

[8] A. Dall'Asta, L. Dezi, Discussion of "Prestress Force Effect on Vibration Frequency of Concrete Bridges" by M. Saiidi, B. Douglas, and S. Feng, Journal of Structural Engineering 122 (4) (1996) 458–458.

[9] A. Kerr, On the dynamic response of a prestressed beam, Journal of Sound and Vibration 49(4) (1976) 569–573.

[10] E. Hamed, Y. Frostig, Natural frequencies of bonded and unbonded prestressed beams - prestress force effects, Journal of Sound and Vibration 295 (1-2) (2006) 28 – 39.

[11] M. Saiidi, B. Douglas, S. Feng, Prestress force effect on vibration frequency of concrete bridges, Journal of Structural Engineering 120 (7) (1994) 2233–2241.

[12] T. Hop, The effect of degree of prestressing and age of concrete beams on frequency and damping of their free vibration, Materials and Structures 24 (1991) 210–220.

[13] Y. Zhang, R. Li, Natural frequency of full-prestressed concrete beam, Transactions of Tianjin University 13 (5) (2007) 354–359.

[14] J.-T. Kim, C.-B. Yun, Y.-S. Ryu, H.-M. Cho, Identification of prestress-loss in PSC beams using modal information, Structural Engineering and Mechanics 17 (3 - 4) (2004) 467–482.

[15] D. Noble, M. Nogal, A. O'Connor, V. Pakrashi, Dynamic impact testing on post-tensioned steel rectangular hollow sections; an investigation into the "compression-softening" effect, Journal of Sound and Vibration [IN REVIEW!] X (2015?) xxx – xxx.

[16] D. Noble, M. Nogal, A. O'Connor, V. Pakrashi, The effect of prestress force magnitude on the natural frequencies of prestressed concrete structures, in: Proceedings of the 23^{rd} Australasian Conference on the Mechanics of Structures and Materials (ACMSM23), Vol. I, Southern Cross University, 2014, pp. 333–338.

[17] D. Noble, M. Nogal, A. O'Connor, V. Pakrashi, Output only investigation of the effect of post-tensioning force on natural frequencies of post-tensioned concrete beams, in: Proceedings of International Operational Modal Analysis Conference IOMAC, International Operational Modal Analysis Conference IOMAC, 2015, pp. xxx–xxx.

[18] British Standards, Eurocode 2: Design of concrete structures Part 1-1: General rules and rules for buildings (December 2004).

[19] D. Noble, M. Nogal, A. O'Connor, V. Pakrashi, Impact hammer testing on post-tensioned steel RHS sections; an investigation of the "Compression Softening" effect, in: Proceedings of Civil Engineering Research in Ireland Conference, Vol. I, Civil Engineering Research Association of Ireland, 2014, pp. 427–432.

[20] D. Foti, V. Gattulli, F. Potenza, Output-only identification and model updating by dynamic testing in unfavorable conditions of a seismically damaged building, Computer-Aided Civil and Infrastructure Engineering 29 (9) (2014) 659–675.

[21] B. Wu, A correction of the half-power bandwidth method for estimating damping, Archive of Applied Mechanics (2014) 1–6.

[22] D. Ho, J. Kim, N. Stubbs, W. Park, Prestress-force estimation in PSC girder using modal parameters and system identification, Advances in Structural Engineering 15 (6) (2012) 997–1012.

[23] B. Peeters, G. De Roeck, One-year monitoring of the z24-bridge: Environmental effects versus damage events, Earthquake Engineering and Structural Dynamics 30 (2) (2001) 149–171.

[24] P. Cornwell, C. Farrar, S. Doebling, H. Sohn, Environmental variability of modal properties, Experimental Techniques 23 (6) (1999) 45–48.

[25] M. S. Williams, S. Falati, Modal testing of a post-tensioned concrete model floor slab, Vol. 1, 1999, pp. 14–20.

[26] Y. Zhang, Y. Zheng, H. Li, A dynamic test of fully prestressed concrete beams, Advanced Materials Research 368 - 373 (2012) 2483–2490.

[27] Z. Lu, S. Law, Identification of prestress force from measured structural responses, Mechanical Systems and Signal Processing 20 (8) (2006) 2186–2199.

[28] S. Jain, S. Goel, Discussion of "Prestress Force Effect on Vibration Frequency of Concrete Bridges" by M. Saiidi, B. Douglas, and S. Feng, Journal of Structural Engineering 122 (4) (1996) 459–460.

[29] C. Bert, Discussion of "Free Vibration Behavior of Prestressed Beams" by K. Kanaka Raju and G. Venkateswara Rao (February, 1986, Vol. 112, No. 2), Journal of Structural Engineering 113 (9) (1987) 2087–2088.

[30] Z. Bažant, L. Cedolin, Discussion of "Free Vibration Behavior of Prestressed Beams" by K. Kanaka Raju and G. Venkateswara Rao (February, 1986, Vol. 112, No. 2), Journal of Structural Engineering 113 (9) (1987) 2087–2087.

[31] F. Bartlett, Discussion of "Free Vibration Behavior of Prestressed Beams" by K. Kanaka Raju and G. Venkateswara Rao (February, 1986, Vol. 112, No. 2), Journal of Structural Engineering 113 (9) (1987) 2085–2087.